J Intell Robot Syst (2011) 61:545–561
DOI 10.1007/s10846-010-9484-x

Solar Airplane Conceptual Design and Performance Estimation

What Size to Choose and What Endurance to Expect

Stefan Leutenegger · Mathieu Jabas · Roland Y. Siegwart

Received: 1 February 2010 / Accepted: 1 September 2010 / Published online: 12 November 2010

Abstract Solar airplanes exhibit a fascination due to their energy sustainability aspect and the potential for sustained flight lasting several day-night cycles. Resulting monitoring and measurement applications at high altitudes but also close to the Earth surface would be extremely useful and are targeted by several research groups and institutions. The question of how to choose the main design parameters of the airplane for a specific mission, considering the current state-of-the-art technologies involved, however, is not easy to answer. A tool is presented performing such a multi-disciplinary optimization. Solar airplanes using both batteries as energy storage devices as well as their capability of flying performance-optimizing altitude profiles can be sized and evaluated in terms of various performance measures. Simulation results show that sustained flight in the Stratosphere is hard to achieve, if the altitude needs to be kept constant. A simulated Remote Control (RC) model size solar airplane allowed to vary altitude proves to be capable of flying multiple day-night cycles at medium and high latitudes during summer.

Keywords Solar airplanes · Conceptual design · Multi-disciplinary optimization · Weight prediction model · Endurance simulation

1 Introduction

Using sustainable energy sources in aviation, be it manned or unmanned, has increasingly attracted scientists around the world. Solar powered flight started in

S. Leutenegger (✉) · R. Y. Siegwart
ETH Zürich, Autonomous Systems Lab,
CLA E 16.2, Tannenstrasse 3, 8092 Zürich, Switzerland
e-mail: stefan.leutenegger@mavt.ethz.ch

M. Jabas
ETH Zürich, Autonomous Systems Lab,
CLA E 25, Tannenstrasse 3, 8092 Zürich, Switzerland

1974 with Sunrise I [3]. The prototype designs of solar-electric airplanes which have been built since then are as manifold as their mission characteristics.

1.1 Examples of Solar-Electric Prototypes

Recently, a first prototype of SolarImpulse [18], took off for the first time: it is supposed to take one person around the Earth using nothing but solar energy. Among the most prominent examples of unmanned solar airplanes, there is NASA's High Altitude, Long Endurance (HALE) series with the huge Helios [10] (75 m wingspan) as its most recent prototype which proved sustained flight in the stratosphere. This goal was also reached by QuinetiQ's Zephyr [14] which is much smaller and lighter (18 m of wingspan and weighing 30 kg): in 2007 it flew for 54 h. These HALE platforms exhibit a large potential as low-cost, more flexible alternatives to satellites. But also airplanes that are deployed closer to the Earth's surface offer interesting observation applications such as early wildfire detection, where long endurance provided by solar energy is favorable. Sky-Sailor, the prototype by ETH of medium Remote Control (RC) model size demonstrated sustained flight in the lower atmosphere in 2008 [12]. Figure 1 shows the aforementioned solar airplanes. A much more exhaustive overview of the history of solar powered flight can be found e.g. in [11].

1.2 Conceptual Design Considerations

When it comes to the conceptual design of solar airplanes, choosing the crucial parameters such as the wingspan that maximize a mission-specific performance measure is a complicated undertaking: the process is highly inter-disciplinary since it involves modeling aerodynamics, environmental characteristics, structural design and assessment of the key technologies such as solar cells and energy storage which undergo rapid progress.

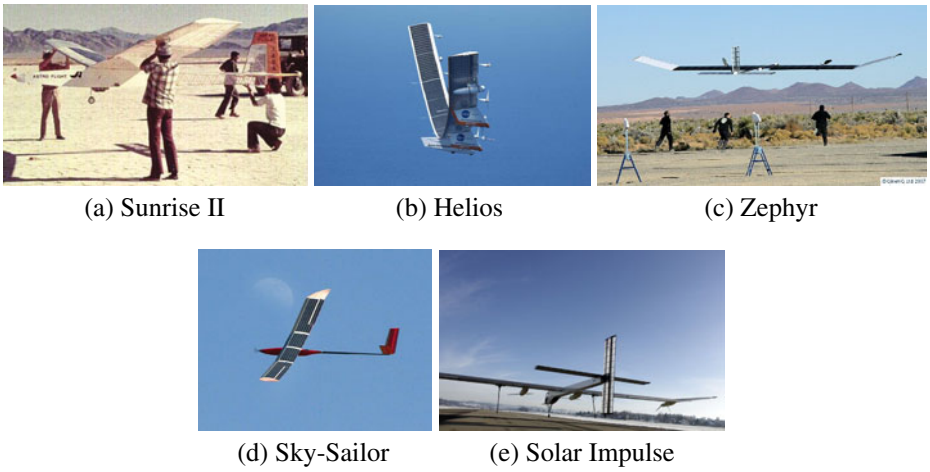

(a) Sunrise II (b) Helios (c) Zephyr

(d) Sky-Sailor (e) Solar Impulse

Fig. 1 Some examples of solar airplanes

Approaches to such multi-disciplinary optimization are provided by various authors. Already in 1974, Irving [9] assessed the feasibility of a manned solar airplane without energy storage capability and concluded that a plane of 25 m wingspan could sustain several hours. Some years later, Phillips [13] treated both potential and electrical energy storage allowing sustained flight in a NASA technical report outlining also the technological advances necessary.

1.3 Overview

In the following, we present a tool for the conceptual design of solar airplanes implemented in MATLAB. It allows simulating missions with various constraints and outputs performance measures which can be optimized. It largely complies with existing tools such as found in [12], differs in the way of modeling the structural mass: rather than basing estimates on statistics, the main design calculations of real feasible lightweight (but simplified) structures are carried out. This implies that mass distributions of scientific payload, propulsion group and energy storage devices that largely influence the necessary structural mass are taken into account. Energy storage in the form of batteries as well in the form of altitude is addressed. The derivation of optimal altitude profiles is carried out with respect to the aforementioned parameters.

In Section 2, an overview of the overall operation of the tool is provided and the meaning of the performance measures is introduced. Section 3 explains the components of the design tool, in particular the structure dimensioning. Section 4 addresses the performance evaluation module. Finally, example results obtained with the tool are shown in Section 5 and discussed.

2 Problem Statement and Overall Operation of the Tool

Before the problem statement can be formulated, some basic concepts need to be explained:

2.1 Endurance and Excess Time

When evaluating the performance of a solar airplane, two different results may be obtained: the aircraft can either be capable of flying theoretically eternally (disregarding change of day duration as the season changes) or not. Figure 2 illustrates these cases and also the direct influence of solar power available, required power and battery energy capacity ($E_{\mathrm{bat,max}}$). For simplification, Fig. 2 only treats flight at constant altitude.

If sustained flight is impossible, the maximum *endurance* ($T_{\mathrm{endurance}}$) will be a reasonable performance measure. However, if it is possible to fly several days, a different measure has to be defined: the *excess time* (T_{excess}) is the time the airplane could still fly in complete darkness after one successful day-night cycle. This measure can therefore be regarded as a safety margin. Notice that $T_{\mathrm{endurance}} > 24$ h does not necessarily imply that sustained flight is possible.

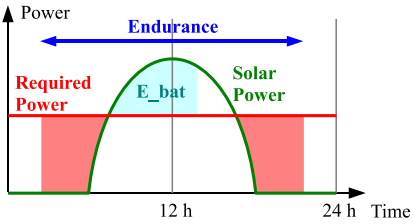

(a) Sustained flight impossible: the maximum endurance is calculated

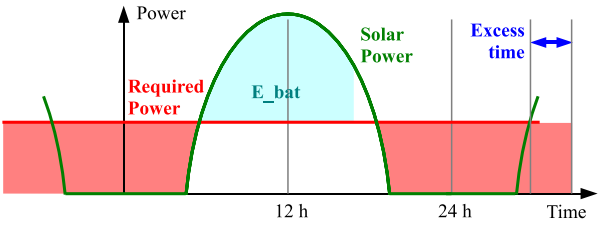

(b) Sustained flight possible: the excess flight time in the morning is calculated

Fig. 2 The influence of solar power, required power and the battery capacity for the two cases where in **a** sustained flight is not possible, but in **b** it is

2.2 Problem Statement, Assumptions and Simplifications

The problem can now be stated as follows: given certain environmental and technological parameters, we want to determine the wingspan b, the aspect ratio Λ and the battery mass m_{bat} that optimize a certain performance measure such as the excess time T_{excess} or the endurance $T_{\text{endurance}}$ of the solar airplane to be designed.

Thereby, some assumptions and simplifications are made:

- In terms of electrical energy storage, only rechargeable batteries are considered featuring a gravimetric energy density which does not depend on the capacity. Right now, Lithium-Ion Batteries are storing approximately 220 Wh/kg, which is the highest value of commercially available cells. The development of higher energy density battery technology is ongoing, e.g. with Lithium–Sulfur cells [17].
- Two simplified structure variants are considered–a rib wing and a shell wing concept that are explained in detail in Section 3.4. These concepts are applicable to lightly loaded wings in the span ranges not far over 10 m. Beyond these values, the correctness of the estimates is supposed to decrease since more efficient structural concepts may be chosen.
- Solar cells of highest power-per-weight ratio are chosen and not varied in the optimization, such as [1]. An efficiency value of 19% is taken at a mass density of 420 g/m^2 including encapsulation. Furthermore, the whole wing surface area is assumed to be horizontal and covered completely with solar cells.

2.3 Overall Operation

Due to the complexity and links between the different components, the tool searches iteratively for optima: the interesting parameters for optimization are clearly the

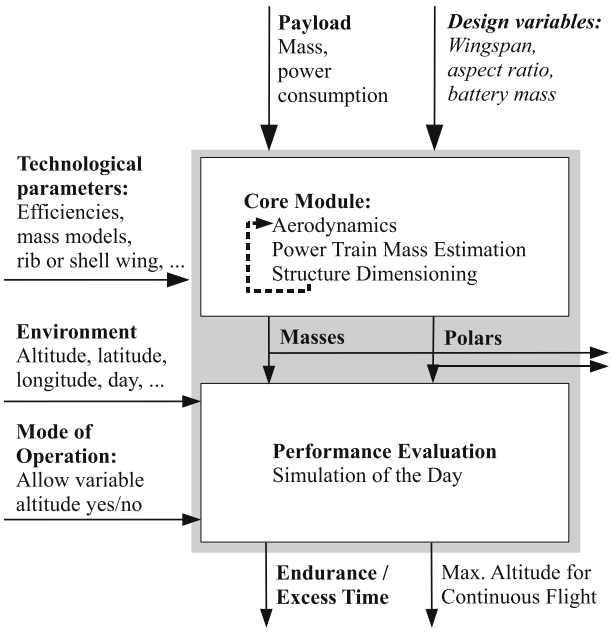

Fig. 3 Overall operation of one iteration loop: the *italic* design variables are to be optimized

wingspan, the aspect ratio and the battery mass. Within one loop, it evaluates the performance of a given configuration. Figure 3 depicts the different components and the respective inputs and outputs. The Core Module inside itself needs to iteratively solve for aerodynamics, power train and structure dimension–which is described in detail in Section 3.4.

This module can now be integrated into a standard optimization framework such as MATLAB's function `fminsearch` , in order to minimize a certain cost function with respect to some of the input variables. Two examples are given in Section 5.

3 Core Module

The Core Module operates as a fix-point iteration on aerodynamics and component masses: It starts with an initial guess of structure mass using the statistical prediction as described in Section 3.4. Next, the aerodynamics associated with different load cases as well as the propulsion group mass are calculated allowing to derive the maximum Shear/Moment/Torque (SMT) loads applied to the various components. This allows calculating the minimum necessary thicknesses of structural elements: both a simplified rib wing and shell wing concept are considered. Finally, the new mass distributions are calculated and the next iteration starts.

In the following, the mentioned sub-modules are described in detail.

3.1 Aerodynamics

For simplification and constraints of computational power, the airfoil is not varied: the MH 139F designed for low power airplanes by Dr. Martin Hepperle was used, the

polars of which were obtained using XFOIL for a wide range of Reynolds numbers. For fast processing, the lift distribution on the main wing is approximated using Schrenk's Method [16]. For the performance evaluation, the induced drag is still estimated as:

$$c_{\mathrm{D,ind}} = \frac{k \cdot c_{\mathrm{L}}^2}{\pi \cdot \Lambda}, \tag{1}$$

where Λ is the aspect ratio and $k = 1.08$ is assumed in order to correct for non-elliptical lift distribution.

Fuselage and stabilizer drag is approximated using flat plate friction with

$$c_{\mathrm{f}} = 0.074 \cdot Re^{-0.2}. \tag{2}$$

At the stabilizers, a conservative assumption of uniform force distribution is made for the loading calculation.

3.2 Power Train

For the dimensioning and weight estimation of the power train, a guess for the necessary power is made using a reasonable choice of the required climbing angle α_{cl} (between 20° for hand launched models and 10° for very large airplanes) at climbing speed v_{cl}:

$$P_{\max} = \frac{1}{\eta_{\mathrm{propulsion}}} \left(v_{\mathrm{cl}} \cdot m_{\mathrm{tot}} \cdot g \cdot \sin \alpha_{\mathrm{cl}} + P_{\mathrm{level}}\right) \tag{3}$$

As described in [12], an estimate for the propulsion group mass based on statistics can now be obtained using

$$m_{\mathrm{propulsion}} \approx 0.0011 \frac{kg}{W} \cdot P_{\max} \tag{4}$$

3.3 Load Cases

On the basis of the European Aviation Safety Agency (EASA) regulations for gliders and motor gliders CS22 [7] as well as on the Unmanned aerial vehicle Systems Airworthiness Requirements (USAR) [19], loads are defined which the structures have to bear. The following operation points define the respective load cases:

- Maximum positive and maximum negative load factors $n_{\max}$ and $n_{\min}$ at manoeuvre speed v_{m}:

$$n_{\max} = 2.1 + \frac{10{,}900}{m_{\mathrm{tot}} + 4{,}536}. \tag{5}$$

- $n_{\max}$ and $n_{\min}$ at dive speed $v_{\mathrm{d}} = 1.5 \cdot v_{\mathrm{m}}$
- ±7.5 m/s gusts at dive speed
- Full aileron deflection (20°) at manoeuvre speed
- Full elevator deflection (30°) at manoeuvre speed
- Full rudder deflection (30°) at manoeuvre speed

The resulting Shear/Moment/Torque loads (SMT) are determined considering the respective mass distribution and load factors as well as roll/pitch/yaw angular accelerations.

3.4 Structure Dimensioning

In the past, several different scaling laws for airplane structures were suggested. Most of them are based on statistics and depend only on a few inputs such as wingspan and aspect ratio Λ. In the design methodology [4], for instance, a proportional relationship of surface (wing, fuselage wetted surface,...) and corresponding weight is taken. The approach of choosing a constant wing loading is also chosen in [15] and other design considerations. Looking at the whole scale range of airplanes, a cubic relationship of weight and scale becomes apparent which is illustrated in Fig. 4 showing Tennekes' [20] Great Flight Diagram which has been augmented with RC sailplanes and unmanned solar airplanes based on [12]. Notice the tremendous statistical variance making it very hard to derive a precise model with only few input variables.

Based on statistics of the lightest 5% of RC model gliders and manned gliders, Noth [12] also found an almost cubic relationship:

$$m_{\text{structure}}(b\,,\,\Lambda) = \frac{0.44\text{N}}{g} \cdot \left(\frac{b}{\text{m}}\right)^{3.1} \cdot \Lambda^{-0.25} \tag{6}$$

This will be used as a starting guess of structural weight by the structure component of the tool.

The methodology described in short here is comparable to [6] and [2], where a real, simplified structure is dimensioned. Mass distributions and load cases are used and heavily influence the resulting structural weight. The downside of this approach is its computational complexity, but at a significant increase of precision.

3.4.1 Rib Wing and Shell Wing Dimensioning

As stated above, the tool calculates two simplified wing structures: cross-sections of a simplified rib wing concept and a shell wing structure are illustrated in Fig. 5, where c is the wing chord length.

The respective thicknesses are dimensioned such that the various specified safety factors and maximum deflections are matched exactly and for a minimal mass. This calculation can be done analytically.

Many practical problems arise before being able to do the calculations associated with the dimensioning, to name the most obvious ones:

- A materials database had to be collected. For the case at hand, measured yield strengths, Young's and flexular moduli for composite materials are used.
- Ratios such as between wing, tail units, fuselage length and also the spacing between the ribs have to be defined. Recommendations are found in airplane design literature.

The automatic structural sizing follows textbook guidelines, mostly found in Hertel's "Leichtbau" [8]. Table 1 lists the main criteria obeyed, each of them yielding associated minimum component thicknesses, of which the largest one has to be selected while still respecting minimum laminate thicknesses. It is noteworthy that both a carbon fiber reinforced (CFR) solution and a glass fiber reinforced version (GFR) is calculated for some components, such that the lighter one can be chosen: at small scale, GFR can in fact be superior.

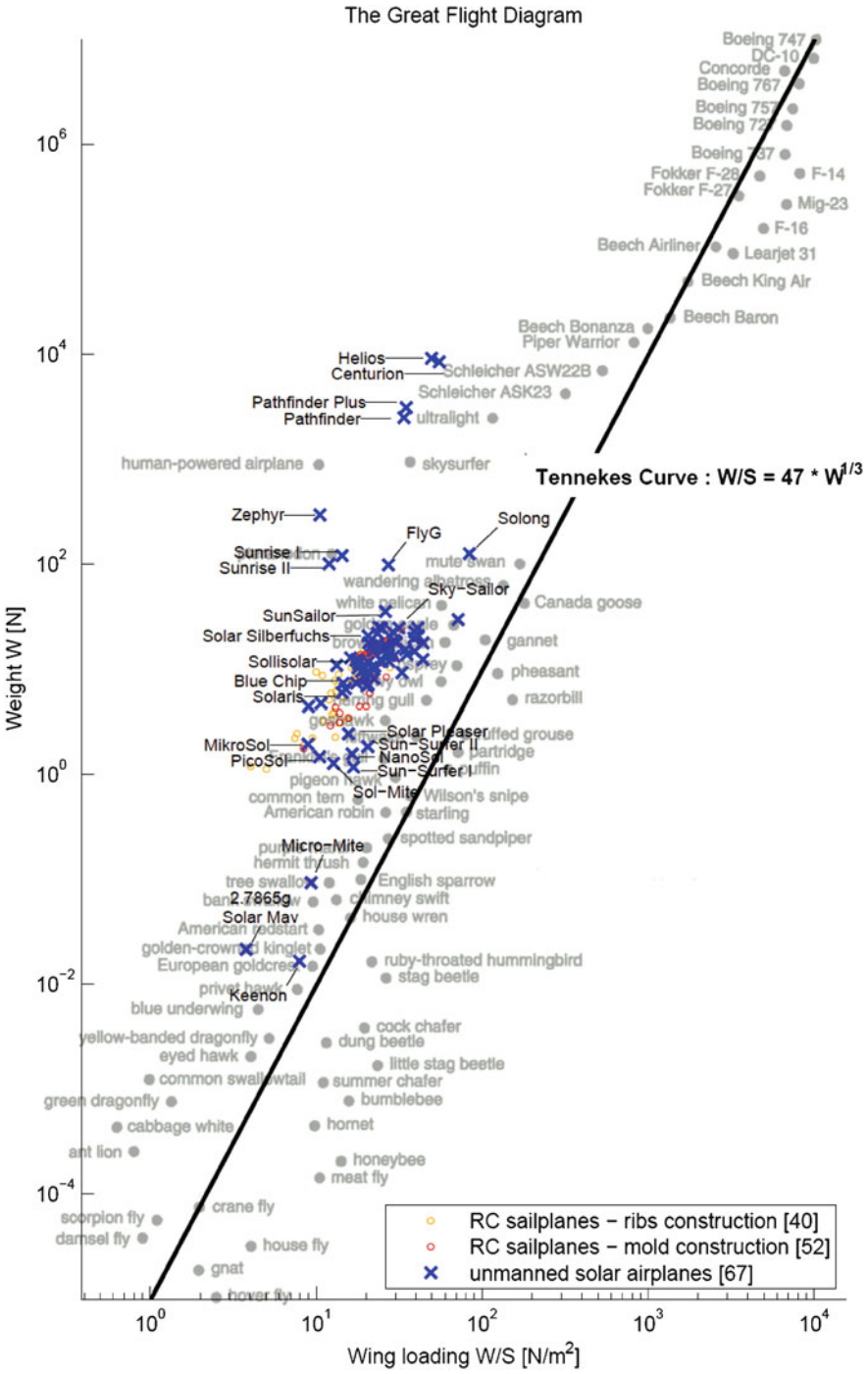

Fig. 4 Tennekes' Great Flight Diagram augmented with some RC sailplanes and unmanned solar airplanes using data collected in [12]

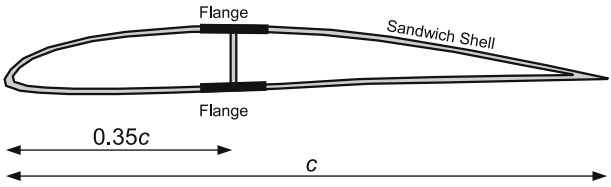

(a) Shell wing concept.

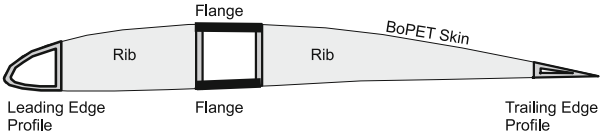

(b) Rib wing concept.

Fig. 5 Two structure concepts used

Providing all equations for the calculation of these different cases would go beyond the scope of this article. Therefore, just the prototype example of shear buckling in the shell is given—other buckling cases are treated in similar manner. Hereby, the thickness of the inner and of the outer laminate $t_{s,tot}$ and the sandwich core material thickness t_{sw} are determined.

First, the maximum torque T_{max} is extracted from the different load cases. Next, the shearflow is calculated according to the Bredt–Batho relation:

$$\tau \cdot t_{s,tot} = \frac{T_{max}}{A_c}, \tag{7}$$

where A_c is the profile cross-section area. The critical stress for non-curved surfaces is obtained with

$$\tau_{crit} = k \cdot E_{corr} \cdot \kappa \cdot \left(\frac{t_{s,tot} + t_{sw}}{0.65c} \right)^2, \tag{8}$$

where $\kappa = 3$ for symmetrical sandwiches, $E_{corr} = E_{1,2,lam} \cdot t_{sw}/(t_{s,tot} + t_{sw})$ is the overall sandwich elastic modulus, $0.65c$ is the longest (almost non-curved) width occurring in the shell and $k = 4.8$ is the buckling factor for the boundary conditions at hand. With a safety factor $S_F = 1.5$, we require $\tau \cdot S_F = \tau_{crit}$. Since the structure

Table 1 Main criteria determining the airplane structure

– Bending of the spar flanges: max. 10° deflection, compression buckling, yield	
Specific to shell wing:	Specific to rib wing
– Shear in the spar web: yield, shear buckling	– Combined shear force and torque in the spar shell: shear buckling, yield, max. 3° twist
– Torsion in the shell: shear buckling, yield, max. 3° twist	– Ribs compression and shear buckling due to aerodynamic forces and skin tension
	– Shear buckling, max. displacement and yield of leading and trailing edge profiles
– Fuselage bending: buckling, yield, max. deflection 2°	
– Stabilizers: identical to main wing	

Table 2 Different mass estimations for some examples

Example	b	Λ	Noth	New	Reality	Remark
Unmanned solar airplanes: rib wing						
Sky-Sailor	3.2 m	12.7	875 g	509 g	700 g	Batt. centered
SunSailor	4.2 m	13.13	2016 g	849 g	1700 g	Batt. centered
Zephyr	18 m	11.6	189 kg	51 kg	≈20 kg	Batt. distr.
Manned solar airplanes: rib wing						
Goss. Penguin	21.6 m	13.86	365 kg	163 kg	31 kg	
Gliders: shell wing (water ballast distributed, pilot centered)						
DG808	18 m	21	163 kg	127 kg	334 kg	
Ventus 2	18 m	23	159 g	135 g	230 kg	

should be of minimum weight, $\rho_{\text{lam}} \cdot t_{\text{s,tot}} + \rho_{\text{core}} \cdot t_{\text{sw}}$ is minimized analytically, with ρ_{lam} and ρ_{core} being the fiber reinforced polymer density, the core material density, respectively.

The resulting equations for the thicknesses are:

$$t_{\text{s,tot}} = \sqrt[3]{\frac{\rho_{\text{core}} S_{\text{F}} T_{\max} (0.65c)^2}{\rho_{\text{lam}} 2 A_{\text{c}} k\kappa E_{1,2,\text{lam}}}} \tag{9}$$

$$t_{\text{sw}} = \frac{S_{\text{F}} T_{\max} (0.65c)^2}{2 A_{\text{c}} k\kappa E_{1,2,\text{lam}} t_{\text{s,tot}}^2}. \tag{10}$$

As stated before, the minimum feasible laminate thicknesses must be respected at least for the outer laminate; an inner laminate can be replaced by appropriately spaced rowings allowing to achieve an arbitrarily low thickness.

3.4.2 Comparison of the Structural Weight Estimation to Real Examples

The described structural sizing and weight estimation is compared to some examples, in order to verify whether the values of the tool are realistic. Both the estimates obtained with the statistical model by Noth and the new model described above are listed in Table 2 for comparison with each-other and with the real structure masses.

The examples illustrate again what the tool was intended for: it gives a baseline for ultra-lightweight airplanes with a wingspan not much over 10 m. Not surprisingly, the two gliders are considerably heavier than the estimates, because they are designed for higher loads, easy handling and not with an extremely weight-optimized structure. The Gossamer Penguin mass, however, is highly overestimated: it is certainly not designed for higher load factors and large aileron deflection at high speed. The same supposedly applies in parts to Zephyr. Nevertheless, the estimates of both the Zephyr as well as the Gossamer Penguin structure mass estimates are considerably closer to the real ones compared to the statistical model.

4 Performance Evaluation

The performance of a configuration is measured as endurance ($T_{\text{endurance}}$ or excess (T_{excess} time as explained above. In some cases, the application may require the

solar airplane to fly at constant altitude, where the performance evaluation is pretty straight-forward and forms a basis. The respective performance values are obtained by simulation of the battery state-of-charge evolution during around a day. If, however, altitude variation is permitted as a means of improving performance due to potential energy storage capability, the respective dynamic optimization problem needs to be solved.

4.1 Environment Model

The solar irradiation is modeled as a function of geographic location, altitude, time and surface normal direction according to [5].

The temperature and air density are estimated using the International Standard Atmosphere. The dynamic viscosity is determined with Southerland's Formula.

4.2 Flight at Constant Altitude

The basics for any considerations is the power needed for level flight at altitude h:

$$P_{\text{level}} = \frac{c_{\text{D}}}{c_{\text{L}}^{3/2}} \sqrt{\frac{2(m_{\text{tot}} g)^3}{\rho(h) A}}. \tag{11}$$

The electrical power required is derived using several efficiencies (of propeller η_{prop}, motor with gearbox η_{mot} and motor controller η_{ctrl}). Finally, the power consumed by avionics P_{av} and by the payload P_{pld} is added:

$$P_{\text{elec,tot}} = \frac{P_{\text{level}}}{\eta_{\text{prop}} \cdot \eta_{\text{mot}} \cdot \eta_{\text{ctrl}}} + P_{\text{av}} + P_{\text{pld}}. \tag{12}$$

On the side of the inflow, the solar power available is derived as a function of the irradiance $I(h, \mathit{latitude}, t)$ follows:

$$P_{\text{solar}} = I \cdot \eta_{\text{sc}} \cdot \eta_{\text{cbr}} \cdot \eta_{\text{mppt}}, \tag{13}$$

where η_{sc} and η_{mppt} are the solar cell and maximum power point tracker efficiencies, respectively. η_{cbr} accounts for solar module level losses mainly caused by camber of the cell arrangement. These losses are typically in the order of 10% [12].

Knowing incoming and spent power, it is straightforward to derive the battery energy state differential equation. It has to be noted that charge and discharge efficiencies are taken into account.

As an alternative performance measure to excess time (T_{excess} of sustained flight at a certain altitude, the maximum altitude for sustained flight can be determined. This is done by a evaluating the performance as described above as a search in the altitude range between 0 and 30 km Above Mean See Level (AMSL).

4.3 Optimal Variable Altitude Profile

Already in [13], altitude profiles are discussed. However, the profiles suggested here look slightly different as will be seen below.

In order to formulate the problem as an optimal control problem with input $u \geq 0$ being the electric power sent to the motor, the dynamics equations can be represented, slightly simplified, in the following form:

$$\frac{dE_{\text{bat}}}{dt} = P_{\text{solar}}(h, t) - u - P_{\text{av}} - P_{\text{pld}}, \tag{14}$$

$$\frac{dh}{dt} = \frac{\eta_{\text{propulsion}} u - P_{\text{level}}(h)}{m_{\text{tot}} g}, \tag{15}$$

with the initial state at t_0 corresponding to the power equilibrium $P_{\text{level}} = P_{\text{solar}}$:

$$h(t_0) = h_0, \tag{16}$$

$$E_{\text{bat}}(t_0) = 0. \tag{17}$$

The following state constraints are imposed:

$$h(t) \geq h_{\min}, \tag{18}$$

$$E_{\text{bat}}(t) \in [0, E_{\text{bat,max}}]. \tag{19}$$

The solar power is forced to still be zero after the night, in order to be able to formulate the problem easily with the partly constrained final state at a fixed t_{end} (not hurting the state constraints):

$$h(t_{\text{end}}) = h_0. \tag{20}$$

And the cost functional to be minimized can be formulated as:

$$J(u(t), h(t)) = -\int_{t_0}^{t_{\text{end}}} \dot{E}(t)\, dt. \tag{21}$$

This can be transformed into

$$\begin{aligned} J(u(t), h(t)) &= \int_{t_0}^{t_{\text{end}}} u - P_{\text{solar}}(h, t) - P_{\text{av}} - P_{\text{pld}}\, dt \\ &= \int_{t_0}^{t_{\text{end}}} \frac{\dot{h}(t) \cdot m_{\text{tot}} g}{\eta_{\text{propulsion}}} + P_{\text{level}}(h) - P_{\text{solar}}(h(t), t) - P_{\text{av}} - P_{\text{pld}}\, dt. \end{aligned} \tag{22}$$

Since the first part is obviously 0, because $h_0 = h_{\text{end}}$ and due to the avionics and payload power consumption P_{av} and P_{pld} being constants, the following simplified cost integral is obtained:

$$\tilde{J}(h(t)) = \int_{t_0}^{t_{\text{end}}} P_{\text{level}}(h(t)) - P_{\text{solar}}(h(t), t)\, dt. \tag{23}$$

Notice that $\tilde{J}$ is only implicitly depending on the control input u. Furhtermore, it can be easily verified that

$$\frac{\partial\big(P_{\text{level}}(h) - P_{\text{solar}}(h,t)\big)}{\partial h} > 0. \tag{24}$$

is valid for all reasonable airplane parameter choices in clear sky conditions. Therefore, the problem can be regarded as always flying as low as possible while still obeying the state constraints. The corresponding optimal trajectory can be formulated easily even as a feedback law:

- Start at $h_0 = h_{\min}$ at the power equilibrium $P_{\text{solar}} = P_{\text{level}} + P_{\text{av}} + P_{\text{pld}}$.
- Fly at the minimum altitude $h_{\min}$. The battery is being charged.
- If $E_{\text{bat}} = E_{\text{bat,max}}$ is reached, choose $u = P_{\text{solar}}(h,t) - P_{\text{av}} - P_{\text{pld}}$, i.e. start climbing using all excess power but not more, the battery stays full.
- As soon as $P_{\text{solar}}(h,t) - P_{\text{av}} - P_{\text{pld}} < 0$, descend with $u = 0$ (gliding mode) down to $h_{\min}$.
- Fly level at $h_{\min}$ until the battery is empty.

A sample profile of a small solar airplane as described in Section 5.2 can be found in Fig. 6.

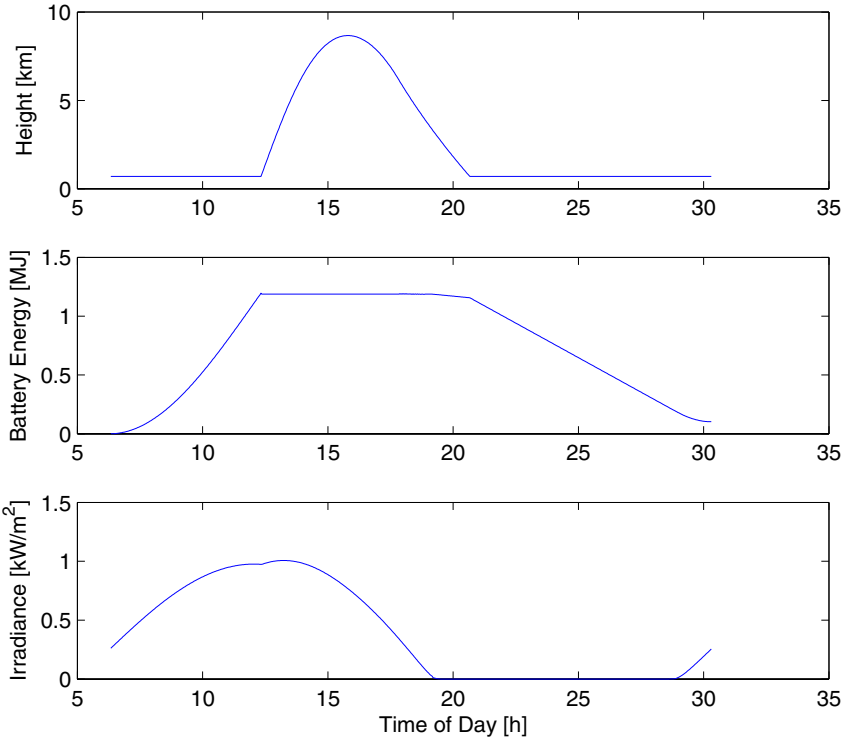

Fig. 6 Altitude, battery energy and irradiation profile of a small solar airplane carrying minimal payload. It can be observed that sustained flight is possible with this airplane in these conditions

5 Simulation Results

5.1 Maximum Constant Altitude for Sustained Flight

A first interesting question that can be answered with the presented tool is the following: how high could a solar airplane fly continuously, during several day-night cycles as a function of latitude given a certain season? And what are the design parameters needed to achieve this? What are the resulting speeds and are these

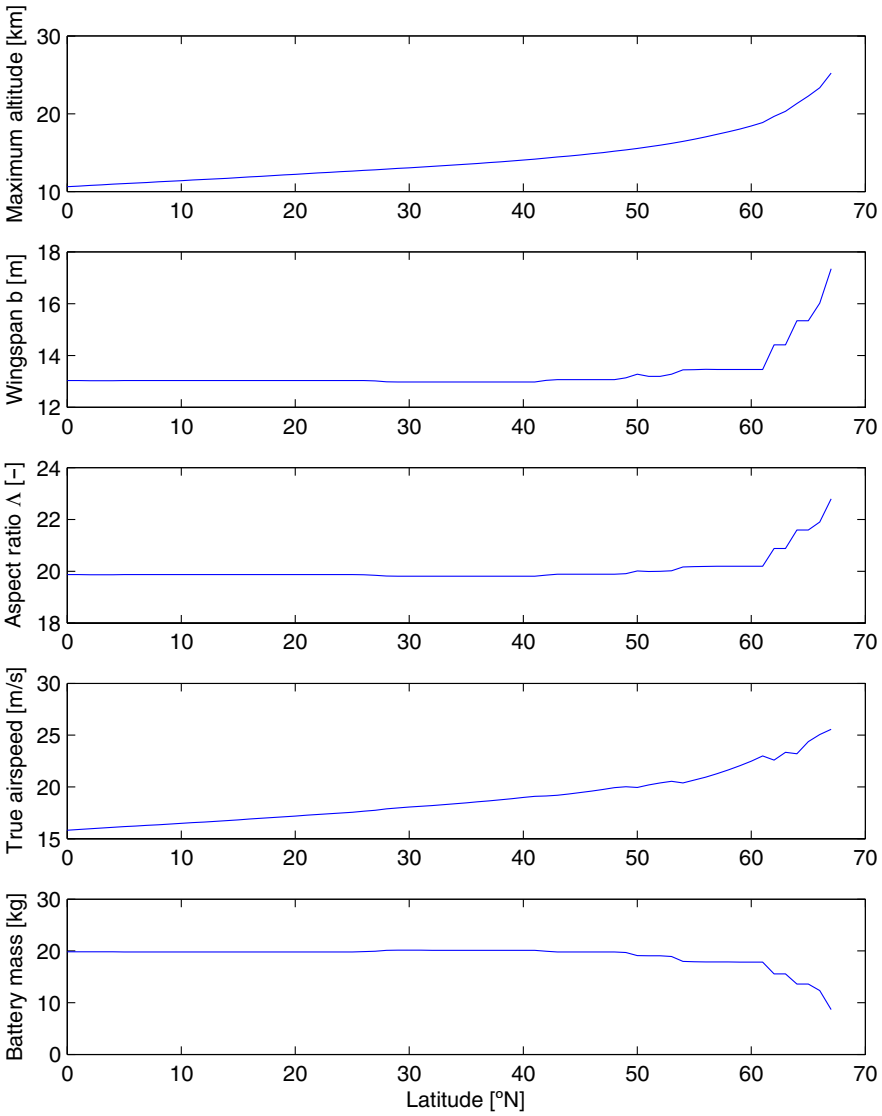

Fig. 7 Maximum constant altitude reachable in sustained flight at summer solstice; corresponding wingspan, aspect ratio, battery mass as well as true airspeed

airplanes going to be able to fly above the tropopause where the sun is not blocked by clouds?

Obviously, the answer to these questions is highly dependent on the payload requirements. A mass of 0.6 kg and a continuous power consumption of 4 W is assumed. This is about the minimum necessary to allow the use of a thermal camera and a minimal data link to a ground station.

Figure 7 summarizes the answers to the questions asked above for the optimal case of summer solstice.

The following points are worth emphasizing:

– The maximum altitude increases smoothly with latitude, but values higher than the tropopause are only achieved north of approximately 40° N.

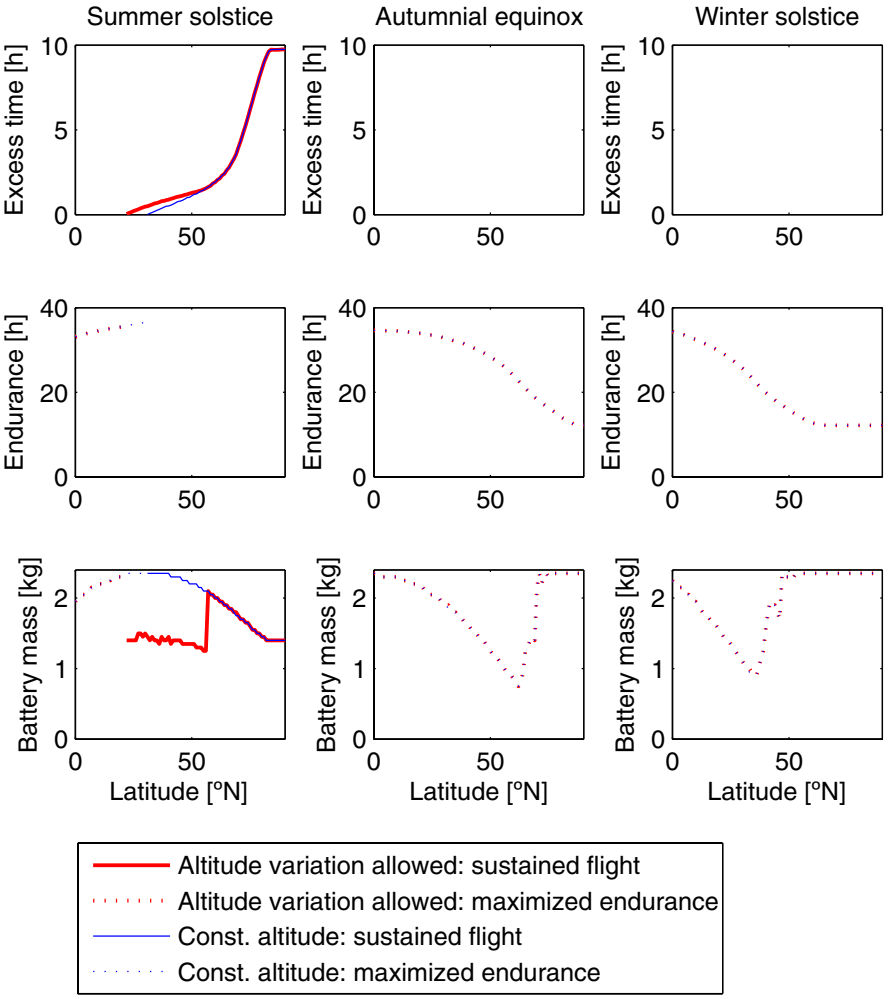

Fig. 8 Performance and optimal battery mass of small solar airplane

- A wingspan b around 13 m and an aspect ratio Λ of approximately 20 seems to be most suitable throughout the interesting band of latitudes.
- The optimal battery mass interestingly also does not vary dramatically as a function of latitude: 20 kg appears to be suitable for most latitudes.
- The true airspeeds of 15–20 m/s are below typical wind speeds in the lower Stratosphere, thus steerability with respect to ground is doubtful in any case.

Unfortunately, even with the spartan payload requirements and at the optimal season, sustained flight at strictly constant altitude above the Tropopause seems to be at the very limit of what is feasible today. Even if it could be achieved (according to the simulation) at higher latitudes in summer, the wind typically blows faster and renders such an undertaking doubtful. Definitely, more advanced large scale solar airplanes using regenerative fuel cells (as in NASA's Helios) for energy storage and/or allowing altitude change would have to be considered in order to achieve better perspectives.

5.2 Performance of a Small Solar UAV

On the other hand, it can be interesting to estimate the maximum performance of a given solar airplane configuration as a function of season and latitude. In the following, a model size airplane is analyzed (3 m wingspan, aspect ratio of 12, design battery mass of 2.35 kg, overall maximum mass of 4.2 kg). Again, a payload of 0.6 kg that consumes 4 W is given–which is considered the absolute minimum necessary to still perform some surveillance task, such as wildfire monitoring using a small thermal camera. The lower altitude limit is set to 700 m AMSL. Figure 8 shows the performance obtained with the design tool in terms of endurance, or, if sustained flight is possible, in terms of excess time.

Notice the following results and interpretations:

- Sustained flight at constant (low) altitude is only possible in summer at medium to high latitudes.
- Allowing variable altitude increases the performance and extends the region of possible sustained flight to lower latitudes. However, the benefits are limited.
- The optimal battery weight changes drastically depending on the environmental conditions and also depending on whether or not altitude variation is allowed.

6 Conclusion

An multi-disciplinary optimization tool for solar airplane conceptual design was presented. One key improvement over existing approaches is the structural module which calculates a feasible simplified structure in order to predict its weight rather than relying on statistical data. Also, flight with variable altitude profile is investigated allowing better performance. The simulation results show that sustained flight at constant altitude with minimal payload can only be performed above the Tropopause at medium to high latitudes in summer and at speeds that are lower than typical wind speeds. The optimal wingspan for such missions are found to be in the range of 13 m. When analyzing an RC-model size solar airplane with a minimal

payload, the simulations show that it could fly sustained in the lower atmosphere at a large range of latitudes that is slightly extended, if altitude variation is allowed.

6.1 Future Work

The integration of more advanced structure concepts valid for larger wingspans together with a less conservative approach of imposing load cases would be of high interest: existing examples of ultra-lightweight solar airplanes show that structural masses can be lower than the presented prediction when scaling up. Finally, it will be interesting to compare the structural and components mass as well as the aerodynamic performance of a new small solar airplane prototype being built to the presented simulations.

Acknowledgements I would like to thank Dr. R. Kickert of Leichtwerk Ing. Buero in Braunschweig, Germany, for his valuable inputs concerning aircraft structure dimensioning and for the fruitful collaboration in the project.

References

1. Azurspace: http://www.azurspace.com/. Accessed 10 Jan 2010 (2009)
2. Berrym, P.: The sunriser—a design study in solar powered flight. In: Proc. of the World Aviation Conference, San Diego, USA (2000)
3. Boucher, R.J.: Project sunrise—a flight demonstration of astro flight model 7404 solar powered remotely piloted vehicle. In: 15th Joint Propulsion Conference, AIAA-79-1264, Las Vegas, Nevada (1976)
4. Brandt, S.A., Gilliam, F.T.: Design analysis methodology for solar-powered aircraft. AIAA J. Aircr. **32**(4), 703–709 (1995)
5. Duffie, J.A., Beckman, W.A.: Solar engineering of thermal processes. NASA STI/Recon. Technical Report A 81(16), 591–+ (1980)
6. Hall, D.W., Hall, S.A.: Structural sizing of a solar powered airplane. Contractor Report 172313, NASA (1984)
7. European Aviation Safety Agency: CS-22, Certification Specifications for Sailplanes and Powered Sailplanes. Available at http://www.easa.eu.int (2003)
8. Hertel, H.: Leichtbau. Springer (1960)
9. Irving, F.G., Morgan, D.: The feasibility of an aircraft propelled by solar energy. In: Proc. of the 2nd International Symposium on the Technology and Science of Low Speed and Motorless Flight, AIAA-1974-1042. Cambridge, MA (1974)
10. Noll, T.E., Brown, J.M., Perez-Davis, M.E., Ishmael, S.D., Tiffany, G.C., Gaier, M.: Investigation of the Helios prototype aircraft mishap. Tech. Rep., NASA Langley Research Center (2004)
11. Noth, A.: History of solar flight. Tech. Rep., ETH Zurich (2006)
12. Noth, A.: Design of solar powered airplanes for continuous flight. Ph.D. Thesis, ETH ZURICH (2009)
13. Philips, W.H.: Some design considerations for solar-powered aircraft. Tech. Rep. 1675, NASA (1980)
14. Quinetiq Newsroom: http://www.qinetiq.com. Accessed 10 Jan 2010 (2006)
15. Rehmet, M.A., Voit-Nitschmann, R., Kröplin, B.: Eine methode zur auslegung von solarflugzeugen. Tech. Rep. DGLR-JT97-031, Universität Stuttgart, Germany (1997)
16. Schrenk, O.: Simple approximation method for obtaining the spanwise lift distribution. NACA TM 948. Available at http://naca.central.cranfield.ac.uk/reports/1940/naca-tm-948.pdf (1940)
17. Sion Power: http://www.sionpower.com/. Accessed 10 Jan 2010 (2009)
18. Solar Impulse News: http://www.solarimpulse.ch. Accessed 10 Jan 2010 (2009)
19. STANAG 4671: Unmanned Aerial Vehicles Systems Airworhiness Requirements (USAR). Nato Standardization Agency (2009)
20. Tennekes, H.: The Simple Science of Flight—From Insects to Jumbo Jets. MIT, Cambridge (1992)